Cloud classification based on histogram analysis of pixel values of night time cloud images over Manila Observatory (14.64N, 121.07E)

*GlennFranco Barroso Gacal[1,2], Nofel Lagrosas[1,2]

1.Manila Observatory, 2.Ateneo de Manila University

Satellites and ground based instruments are utilized to achieve cloud detection. At night time, detection of clouds is accomplished by satellites, whole-sky imagers, lidars, and sky cameras. In practice, ground-based detection is executed by sky cameras and whole-sky imagers and incorporating a threshold value into the analysis of cloud detection. This will classify pixels as clouds or non-clouds. In this work, we use a ground-based sky imager using a digital camera to take pictures of the sky. The digital camera (Canon Powershot A2300) is continuously operated to take images of night time clouds at 5 minute intervals. The camera is configured to have an exposure time of 1s and 5s and is situated on the roof top of the Manila Observatory building (14.64N, 121.07E). This is to ensure that there is a minimal presence of obstructions for the camera. A threshold value is applied to distinguish a pixel to be a cloud or non-cloud by analyzing the histogram of pixel values of clear sky. Other works use the similar procedure of applying a threshold value to detect clouds at daytime (Heinle et al., 2010). In this study, the RGB formatted images are converted to greyscale format. Lastly, an algorithm is applied to compute cloud occurrence (Gacal et al., *submitted*). Cloud occurrence is determined but not its corresponding cloud types: thin, thick, and cloud-free. The objective of this study is to determine these cloud types in terms of their range of pixel values. Figs. 1a -1c show the images of a clear night sky, thin clouds, and thick clouds, respectively. These images were taken on 16 January 2016, 21 October 2015, and 25 May 2014, respectively. From visual inspection, thick clouds (Fig. 1c) are perceived to have no distinguishable dark background as compared to the thin clouds (Fig. 1b). Figs. 1a –1c are taken at 1s exposure time except Fig. 1a with an exposure time of 5s. Figs. 1d –1f show the histogram of each corresponding cloud type. The histogram of a cloud free sky (Fig. 1d) presents the pixel values that range from 0 –16. This implies that a minimal pixel value of 17 can be used to discriminate the presence and absence of clouds of a night sky (Gacal et al., *submitted*). Comparing this to Fig 1e, this histogram shows a superposition of a clear sky and thin clouds. Since the range of pixel values for a clear night sky is from 0 –16, it follows that the remaining range of pixel values has to be from thin clouds. In this study, we observe that the range of pixel values for thin clouds is from 19 –40. Fig. 1f is a histogram of an extreme example of a thick cloud where pixel values range from 47 –111. Visual inspection of Fig 1c shows that there is no thin cloud or clear sky component. This pixel range can represent of thick clouds at night time. This work has shown the possibility of discriminating cloud types in terms of the range of pixel values. In the future, these results will be used to calculate cloud cover from thin and thick clouds as the calculation of cloud occurrence is simultaneously done.

References:

Heinle, A., Macke, A., Srivastav, A. (2010). Automatic cloud classification of whole sky images. *Atmos. Meas. Teach*, 3: 557-567.

Gacal, G.F.B., Antioquia, C., Lagrosas, N. (2016). Ground-based cloud detection of night time clouds above Manila Observatory (14.64N, 121.07E) using a digital camera. *Aerosol and Air Quality Research. (submitted).*

Keywords: Digital image, Pixel values, Histogram, Nighttime clouds

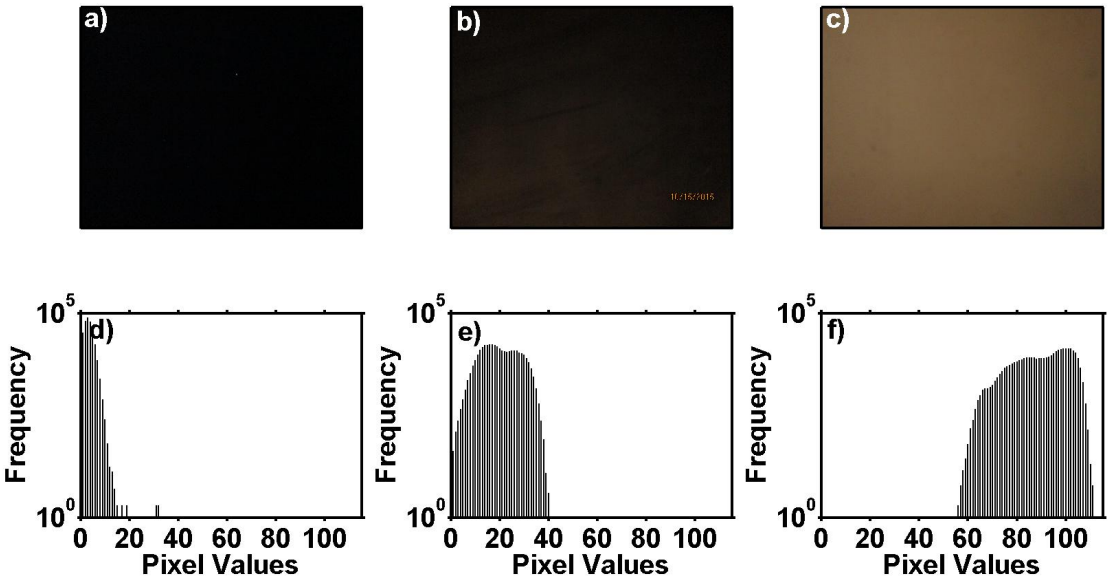

Observations of night time cloud cover sensitivity measurements with changes in threshold pixel values

*Nofel DelaCruz Lagrosas[1,2], Glenn Franco Barroso Gacal[1,2]

1.Manila Observatory , 2.Ateneo de Manila University

Detection of night time clouds is carried out in Manila Observatory (14.64N, 121.07E) for the purpose of measuring cloud cover at night time since late of 2014. A digital camera (Canon A2300 Powershot) is used to take images of sky every 5 minutes. Images are taken at 5s exposure time. The digital images, which are in standard RGB format, are converted to grayscale format for cloud detection analysis. Cloud detection is possible by setting a threshold pixel value that discriminates clear from cloudy sky. Previous study has shown that a threshold pixel value of 17 can be used for cloud detection (Gacal, et al, 2014). Cloud cover is defined as the ratio of the sum of the number of pixels identified as having cloud signals to the sum of the total number of pixels in the image. Cloud cover measurement has impacts on the radiation budget in the atmosphere even during night time. High cloud cover of thick clouds covering majority of the sky tend to reflect back radiation from the earth's surface. Thin clouds, on the other hand, may transmit earth's radiation to space and reflect less. In an ordinary image of night sky, the image may contain thick and thin clouds. In this work, we define a thick cloud in the image as cloud without any clear dark background. The images of thin clouds have visible dark background. For the purpose of quantifying cloud cover from thin and thick clouds, we present in this study the effects of varying threshold pixel value used in cloud detection algorithm on the calculation of night time cloud cover. Figs. 1a-c show images of clear sky, thin cloud and thick clouds taken on 12 January 2016 at 03:05, 22 December 2015 at 05:40 and 16 January 2016 21:15 local time, respectively. Local time is 8 hours ahead of coordinated universal time (UTC). Histogram of pixel values of clear sky image shows that maximum pixel value is 16 and can be used as a threshold value for discriminating clear from cloudy skies in the cloud detection algorithm. When this threshold value is changed from 10 to 40, cloud cover values also change. At threshold pixel value of 10, cloud detection algorithm applied to clear sky outputs ~3% cloud cover but rapidly decreases to zero for higher pixel values (Fig. 1d). When the algorithm is applied to thin cloud image, a sharp decrease of cloud cover values is observed for threshold pixel value > 20 but almost 100% cloud cover for threshold pixel value < 20 (Fig. 1e). From visual inspection of the image, a near 100% cloud cover is evident. The near exponential decrease of cloud cover values is a common characteristic when threshold pixel value is changed for images with thin clouds. Thus, without any idea of the image, this exponential decrease of cloud cover trend can be used to indicate that the image is dominated by thin clouds. When threshold pixel values are changed in the cloud detection algorithm and applied to images with thick clouds, the decrease of cloud cover values is not as sharp as in the case of thin clouds. Fig. 1f shows the non-exponential decrease of cloud cover values with threshold pixel value change. The graph shown is Fig. 1f is also a characteristic graph for thick clouds. Thus, the non-exponential decrease can be used for determining presence of thick clouds in the image without inspecting at the image. Images of rain clouds are extreme examples of thick clouds. When images of these types of clouds are processed using the same algorithm and changing threshold pixel value from 10 to 40, resulting cloud cover values do not change and are at 100%. This is expected since pixel values of thick clouds are usually in the range of 47 to 111.

Keywords: Night time clouds, Pixel value, Cloud cover

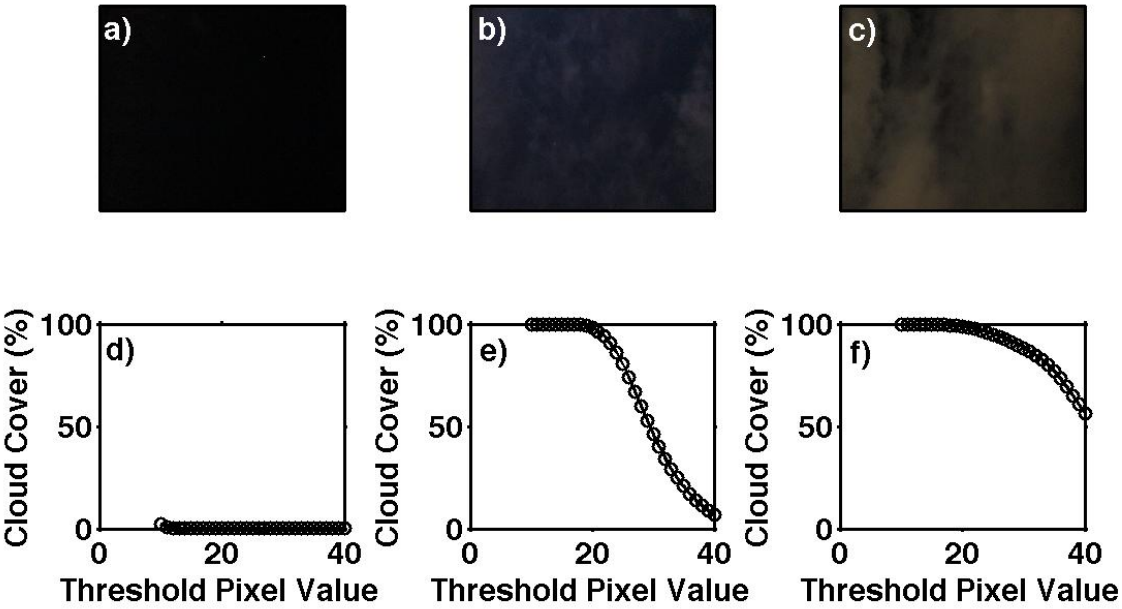

Three dimensional structure of the Arctic cyclones

*Takuro Aizawa[1], Hiroshi L Tanaka[2]

1.Graduate School of Life and Environmental Sciences, University of Tsukuba, 2.Center for Computational Sciences, University of Tsukuba

Arctic cyclones are unique low pressure systems appearing in the Arctic, which are different from the tropical cyclones and the mid-latitude cyclones. Previous studies provided a new insight that the surface Arctic cyclone connects to an upper polar vortex producing a deep barotropic vortex. The previous studies also noted that the characteristic thermal and the vortical structures are maintained throughout a life cycle. But, the three dimensional stereoscopic structure of the Arctic cyclones was not investigated by the previous studies.
To investigated the three dimensional structure of the Arctic cyclones, we converted the meteorological data from a latitude/longitude coordinate system into the cylindrical coordinate system around the Arctic cyclone center. The original data used this study are the reanalysis data of JRA-25 (Japanese 25year Reanalysis) and JRA-55 (Japanese 55year Reanalysis).
The Arctic cyclone has a deep barotropic cyclonic circulation, a secondary circulation in the troposphere, a downdraft at the lower stratosphere, a coupling of a warm core at the lower stratosphere and a cold core in the troposphere, and a deep tropopause folding over the cyclone center.
For the Arctic cyclone, the positive relative vorticity related to the deep axisymmetric cyclonic circulation stretches up to the stratosphere of 50 hPa level from the surface indicating a connection with the stratospheric polar vortex. The upper vortex of the well-developed occluded cyclone is not the polar vortex in the stratosphere. The Arctic cyclone at the surface is characterized by the deep stratospheric polar vortex, which is a different from the occluded cyclone in terms of the vertical scale.
Although additional studies are needed, a schematic diagram of the Arctic cyclone is proposed in this study.

Keywords: Primary circulation, thermal structure, polar vortex

An anaysis of fine structure in the summer troposphere and stratosphere based on radiosonde observations at Shigaraki, Shiga, Japan

*Yuta Mizutani[1], Shota Sugano[1], Yuki Kawata[1], Kaoru Sato[2]

1.Dept. Earth and Planetary Physics, School of Science, The University of Tokyo, 2.Department of Earth and Planetary Science, The University of Tokyo

In order to examine characteristics of atmospheric fine structure in the troposphere and stratosphere, radiosondes were launched every 3 hours from 18:00JST 27th July,2015 to 18:00JST 28th at Shigaraki MU Observatory, Kyoto University. Vertical profiles of horizontal wind, temperature, and relative humidity were obtained at a height interval of 5 m. During the observation period, high and low pressure systems are situated in the south and north of Japan, respectively. This is a typical synoptic-scale pressure pattern in summer in Japan. The tropopause determined based on the Brunt-Vaisala frequency was located around a height of 15 km. Using these observation data, time evolution of the atmospheric boundary layer, altitude dependency of dominant vertical wavelength, and dynamic characterictics of dominant wave-like structure in the stratosphere were analyzed.
First, we examined in detail the vertical profiles of the potential temperature, the equivalent potential temperature, and water-vapor mixing ratio to see development of the atmospheric boundary layer in daytime. It is expected that these quantities are constant in the vertical as a result of strong convection in the mixing layer. The altitude up to which these quantities are constant was raised from 0.5 km to 1.2 km during the time period of 9:00-15:00LST. On the other hand, a strong inversion layer appeared in the lowermost troposphere at 3:00LST.
Second, a wavelet analysis with a box-car type mother wavelet was carried out. The wavelet spectrum for each vertical profile of temperature, zonal wind, and meridional wind was calculated, and the mean spectrum for the entire period was obtained. It was clear that dominant wavelength depends on the altitude. It is approximately 1 km and 6 km for the lower (15-25 km) and middle (25-35 km) stratosphere, respectively. Because any drastic change in the Brunt-Vaisala frequency and background winds were not observed, it is inferred that the disturbance with the long vertical wavelength in the middle stratosphere was generated in the region far from, propagated horizontally toward and reached the observatory.
Phases of the dominant wave propagate downward, suggesting that the disturbance is due to an internal gravity wave propagating energy upward. Given a working hypothesis that the wave disturbance was an internal gravity wave, a hodograph analysis was carried out. First, the background wind was obtained as a linear least square fit for the vertical profiles of zonal and meridional winds above a height of 20 km. Deviation from the background wind was analyzed as the disturbance component. The hodograph of the disturbance component was approximated by an ellipse. The intrinsic frequency was estimated from the ratio of long to short axes of the ellipse. The horizontal wavenumber was determined from the dispersion relation of the internal gravity wave, using the estimated intrinsic frequency and the vertical wavenumber directly obtained from the vertical profile. The ground-based frequency that was determined from these wave parameters and the mean wind was approximately consistent with that observed in the time series of the vertical profiles. This means that the working hypothesis was valid and that the disturbance is due to an internal gravity wave. Furthermore, using these wave parameters and the mean wind, and the propagation paths of the internal gravity wave was estimated. As a result, it was concluded that the gravity wave likely originated from the low pressure system over a northern part of Korean Peninsula.

Keywords: radiosonde observations, wavelet analysis, internal gravity waves

Changes in the lower stratospheric residual circulation in JRA-55

*chiaki Kobayashi[1]

1.Meteorological Research Institute

Future projections by many climate models suggest that the Brewer-Dobson circulation (BDC) will be intensified as a result of rising greenhouse gas concentrations. However, observations show a diversity of the BDC strength changes. In this study, we investigate the changes in the BDC using JRA-55 reanalysis data compared with JRA-55-related products. In JRA-55, the annual mean tropical upwelling shows a significant increasing trend in the lower stratosphere from 1979 to 2012. JRA-55C also indicate a significant increasing trend of the upwelling, but JRA-55AMIP does not. These BDC strengths are assessed by climatological zonal mean which is removed diurnal variations.
Recently, Sakazaki et al (2015) found zonally uniform tidal signals in the tropical stratosphere. The vertical wind diurnal amplitudes in the lower stratosphere is not a negligible amount compared with climatological upwelling.
The BDC trend in JRA-55 linked with the representation of the tidal signals change related to the observing system changes in the reanalysis. Comparison of the relation among the JRA-55 family members is discussed in the presentation.

Keywords: JRA-55, Brewer-Dobson circulation, lower stratosphere

Characteristics of the polar vortex and the AO index in the upper stratosphere and lower mesosphere in Arctic winter II

*Kazuyo Sakanoi[1], Takenari Kinoshita[2], Kaoru Sato[3], Yasuhiro Murayama[2]

1.Komazawa University, 2.NICT, 3.The University of Tokyo

Purpose of this research is to clarify relationship between solar activity and disturbance in the middle atmosphere during Arctic winter. In this research we consider stratospheric sudden warming (SSW), which is a typical phenomenon in Arctic winter, as disturbance in the middle atmosphere including the mesosphere. Previous research [ex. Labitzke, 2005] reported effect of 11-year solar cycle on thermal structure only in the Stratosphere.
Traditional classification of SSW is not suited for quantitative comparison with other indices. Therefore we are exploring new indices which display condition of disturbance in the mesosphere. In this presentation, we calculate AO index in the altitude range from 1000 hPa to 0.1 hPa (65km alt) in 1999/2000 -2007/2008 winters. AO index also represents well the degree of disturbance in the middle atmosphere. We also use 2D vortex moment diagnostics (Z10 method) [Seviour et al., 2013] to check condition of the polar vortex at 10 hPa and 0.316 hPa. The results of these analysis is summarized as follows:
> The peak altitude of AO index is about 0.5 hPa.
> Positivity/negativity of AO index is almost coincident at 100 hPa -0.1 hPa.
> High negative value and negative AO index in all altitude are not necessarily required in Major Warmings.
> Wave 1 and 2 configuration are observed at 10 and 0.316 hPa in Major Warmings and comparable level events. Strong wave 1 is exists especially in 10 hPa.
> Wave 1 and 2 configuration are observed at 0.316 hPa in minor Warmings. At 10 hPa there are no disturbance or wave 2 configuration.
> Negative AO is shown in all altitude range when strong wave 2 exist at 10 hPa.
References:
Labitzke, K. (2005). On the solar cycle-QBO relationship: A summary. Journal of Atmospheric and Solar-Terrestrial Physics, 67(1-2), 45-54. http://doi.org/10.1016/j.jastp.2004.07.016
Seviour, W. et al. (2013). A practical method to identify displaced and split stratospheric polar vortex events. Geophysical Research Letters, 40(19), 5268-5273. http://doi.org/10.1002/grl.50927

Keywords: Stratospheric sudden warming, Arctic, Mesosphere

Dynamical response of the SH middle atmosphere to energetic particle precipitations in the latest reanalysis data

*Yoshihiro Tomikawa[1,2]

1.National Institute of Polar Research, 2.SOKENDAI

The latest solar cycle minimum sometime around 2009 showed unusually low solar activity and suggested the possibility of a grand solar minimum in the near future. This event caused much attention to be focused on studies regarding solar influence on the Earth's climate. The recent review by Gray et al. (2010) classified solar forcing on the Earth's climate to be of four types: galactic cosmic rays, total solar irradiance (TSI), solar ultraviolet radiation (UV), and energetic particle precipitations (EPP). Although EPP has not attracted much attention compared with TSI and UV in the past, several recent studies indicate that EPP could have a significant impact on the Earth's climate, comparable with that of TSI and UV. However, reliability of some of these studies was recently questioned (Tomikawa, 2015). In this study, the past 36 years were divided into high, medium, and low energetic particle forcing (EPF), and solar maximum, medium, and minimum conditions using Ap index and F10.7 radio flux, respectively. Then composite figures of middle atmosphere in the winter southern hemisphere were created from the latest reanalysis data and compared between medium and low EPF during the solar minimum. They showed that there was a statistically significant difference between medium and low EPF.

Keywords: Energetic particle precipitation, Reanalysis, Middle atmosphere

An observation of the mesospheric column amount of nitric oxide observed with a millimeter-wave spectral radiometer at Syowa station in Antarctica

*Tomoo Nagahama[1], Akira Mizuno[1], Tac Nakajima[1], Hirofumi Ohyama[1], Yasusuke Kojima[1], Mitsumu K. Ejiri[2], Yoshihiro Tomikawa[2], Masaki Tsutsumi[2], Takuji Nakamura[2]

1.Institute for Space-Earth Environmental Research, Nagoya University, 2.National Institute of Polar Research

Since 2011, the ISEE and NIPR started a joint research project on monitoring the composition changes in mesosphere and lower thermosphere (MLT) by using a millimeter-wave spectroscopy technique, and installed a millimeter-wave spectral radiometer with a high-sensitivity superconducting (SIS) mixer receiver operated in 250 GHz band at Syowa station in Antarctica (69°S, 40°E) for measuring the emission spectrum of nitric oxide (NO) in January 2012. The partial column of NO ranging from 75 to 100 km in altitude is retrieved from the observed emission spectrum. The mesospheric chemical composition largely varies caused by environmental changes of the earth inside and outside. Recent studies reported enhancement of NO_x and HO_x and ozone depletion in the polar mesospheric region caused by precipitating the energetic particles such as a solar proton and an electron in the radiation belt (e.g., Andersson et al. 2014). From the dataset observed with the radiometer in more than 4 years, we find that the NO column amount shows the maximum in winter, but the peak amount in 2014 is about a half of those in other years. In addition, we detect sporadic enhancement of the NO column amount during a few weeks in June, August and October of 2015 that may be associated with solar activity. In the presentation, we report the features of temporal variations of the observed NO column amount as well as the detail comparison with physical properties of precipitating solar protons and the electrons from the radiation belt.

Keywords: mesosphere, atmospheric composition change, millimeter-wave measurement

Influences of QBO and solar cycle on the Arctic ozone

*Yousuke Yamashita[1], Hideharu Akiyoshi[1]

1.National Institute for Environmental Studies

The quasi-biennial oscillation (QBO) and the solar 11-year cycle are known to cause year-to-year variability of the Northern Hemisphere (NH) polar vortex (e.g., Holton and Tan, 1980; Labitzke and van Loon, 1988). Yamashita et al. (2015) indicated that the polar vortex is strong in early winter and weak in late winter for the westerly phase of the QBO (QBO-W) and solar maximum (S_{max}) years. In contrast, the polar vortex is strong from early to late winter for the QBO-W and solar minimum (S_{min}) (QBO-W/S_{min}) years, implying the small Arctic ozone in late winter. Li and Tung (2009) found that the observed Arctic total ozone in March is the smallest in magnitude for the QBO-W/S_{min} years. In this study, the influences of QBO-W/S_{min} on the Arctic ozone in late winter are analyzed from outputs of a chemistry climate model (CCM) in which the meteorological fields of the model are nudged toward the observational data for 1979–2011. The strong polar vortex relative to the climatology is shown in February–March during QBO-W/S_{min}. The minimum of Arctic total ozone is simulated during the QBO-W/S_{min} condition in February–March, in agreement with the satellite observations. We also analyze the total ozone derived from passive ozone tracer that is simply advected without any chemical change. The results of the passive ozone tracer show the similar results of the original total ozone, suggesting the prominence of transport change of ozone for the minimum total ozone under the QBO-W/S_{min} condition in February–March. The further analysis of the vertical structure suggests that while the minimum of Arctic total ozone is mainly explained by the transport change of ozone around 100–200 hPa, the enhancement of chemical destruction of ozone due to the low temperature within the polar vortex observed around 20–50 hPa under the QBO-W/S_{min} condition is partly related to the local ozone depletion around 20–50 hPa.

Keywords: quasi-biennial oscillation, solar 11-year cycle, Arctic ozone

A global analysis of seasonal total ozone trend for the CFC increase period using TOMS data and the MIROC3.2 nudged Chemistry-Climate Model

Risa Obama[1], *Hideharu Akiyoshi[1], Yousuke Yamashita[1], Masanao Kadowaki[1]

1.National Institute for Environmental Studies

In this study, we globally analyzed seasonal total column ozone trends for the period 1979-1993 and 1979-1997. We compared the total ozone trends of a nudged CCM with those of TOMS. The nudged CCM is the MIROC3.2 Chemistry-Climate Model nudged toward ERA-Interim reanalysis data. The comparison showed that the model simulation reproduced well the trends globally. In order to separate the effects of ozone changes due to the chemical reactions and the transport on the trends, we performed a 1979-ODS experiment, in which ODS concentration was fixed to the 1979 value. The results indicate that chemical ozone loss is more dominant as a driver of the trends than ozone transport change at the mid-latitudes in the Southern Hemisphere, whilst at the mid-latitudes in the Northern Hemisphere ozone transport is more dominant than the chemical loss in the winter and spring, and both the effects are comparable in the summer and autumn. From a global ozone trend map, we show significant negative trends over the Pacific Ocean in the east of Japan, around the east coast of the North America, and over Europe. These trend distributions suggest some effect of planetary scale wave activitiy change in the Northern Hemisphere winter and spring for the CFC increase period.

Keywords: total ozone, long-term trend, nudged Chemistry-Climate Model, TOMS, ERA-Interim

Variations of stratospheric and tropospheric circulations related with ozone hole

*MASAAKI NAKAMURA[1], MASAAKI TAKAHASHI[2], HIDEHARU AKIYOSHI[3], Yousuke Yamashita[3]

1.Mitsubishi UFJ Research and Consulting, 2.Atmosphere and Ocean Research Institute, University of Tokyo, 3.National Institute for Environmental Studies

Due to anthropogenic emissions of ozone depleting substances, ozone hole has been developing in Antarctic stratosphere during the spring since about the 1980s. Ozone absorbs incoming solar radiation and heating the stratosphere. Hence the depletion of ozone over Antarctica leads to cooling of the polar stratosphere. As a result, polar vortex is strengthened from thermal wind equation. These variations related with ozone hole appear only in Antarctic stratosphere during the spring so that it was considered that the ozone depletion does not affect tropospheric climate. Since about the 2000s, however, it has become clear that the ozone hole is also associated with widespread changes in the Southern Hemisphere tropospheric circulation and surface climate. Previous research studies showed that the influences of the ozone hole go down from stratosphere and appear lower troposphere during the austral summer season. This tropospheric variation pattern resembles the most prominent pattern of large-scale Southern Hemisphere climate variability, the Southern Annular Mode. Hence the influence of the ozone hole has led to a range of Southern Hemisphere climate changes not only Antarctic stratosphere, but also over the Southern Hemisphere troposphere. However the mechanism of influence from the stratosphere to the troposphere is unclear. This study revealed how the stratospheric variation related with ozone hole affect the troposphere during austral summer season.

Previous study analyzed this mechanism using monthly or seasonal data; therefore, variations with timescale shorter than a month cannot be analyzed. For this reason, we used 10 days mean data in order to research the detail of the mechanism in the austral summer. As a result, we found out the variations of eastward wind are different among December, January and February. In December, most of eastward wind variations occur in the stratosphere and upper troposphere. In January, stratospheric variations disappear and only tropospheric variation can be found. In February, we could not find any significant variations both stratosphere and troposphere. We tried to find out the reason why these different variations appear using EP-Flux. As a result, we realized that, in December, wavenumber 1 propagating into the stratosphere has the most important role and that baroclinic instabilities with wavenumber 4 and 6 are important in January.

Furthermore we studied the influences of both global warming and ozone hole on Southern Hemisphere climate. We investigated in the Chemical Climate Model based on MIROC 3.2 using three scenarios, one is reference simulation, another is sensitivity simulation which is similar to reference simulation, but halogens fixed at 1960 levels throughout the simulation, and the last is sensitivity simulation which is also similar to reference simulation, but GHGs fixed at 1960 levels. Hence we can discuss two influences both global warming and ozone hole on Southern Hemisphere climate variations separately. As a result, we realized ozone hole has a role to maintain the signal at the lower troposphere in austral summer. On the other hand, global warming makes Brewer-Dobson circulation strong and the transportation of ozone to polar region is also enhanced. Because of ozone heating, global warming has a role to warm the polar atmosphere. Previous studies notice only the GHGs`s radiative cooling in the stratosphere but we suggested that the change of physical field is also important in the variation of Southern Hemisphere climate.

Un-volatile aerosol layer in the lower most stratosphere over tarawa, Kiribati, observed bu balloon norne Optical Particle Counter in january, 2016

*Masahiko Hayashi[1], Naomi Eguchi[1], Koichi Shiraishi[1], Yoichi Inai[2], Satoru Mimura[2], Fumio Hasebe[2], Takashi Shibata[3]

1.Faculty of Science, Fukuoka University, 2.Hokkaido University, 3.Nagoya University

Size distributions and volatility of aerosols in the Tropical Tropopause Layer (TTL) over Tarawa (1.5 °S, 173.0 °E) were observed using balloon-borne dual optical particle counters (OPC) in January 2016. One OPC observed number concentration of ambient aerosols and another OPC observed aerosol size distribution denuded at 200 °C, in order to discuss volatility of aerosls.
Unusual aerosol layer was found in the stratosphere from 18 to 22 km in altitude. The layer was divided into two sub-layers. Upper layer was characterized by smaller high volatile aerosol, and lower one by mixture with larger submicron un-volatile aerosol. The feature was similar to fresh volcanic aerosol layer, however we did not find any report of large volcanic eruption in 2015. We will discuss about origin of the layer.

Keywords: Tropical Tropopause Layer, stratsphere, aerosol, volatility

